

1 Towards a Pixel TPC part I: construction and test of a
2 32 chip GridPix detector

3 M. van Beuzekom^a, Y. Bilevych^b, K. Desch^b, S. van Doesburg^a,
4 H. van der Graaf^a, F. Hartjes^a, J. Kaminski^b, P.M. Kluit^a, N. van der Kolk^a,
5 C. Ligtenberg^a, G. Raven^a, J. Timmermans^a

6 ^a*Nikhef, Science Park 105, 1098 XG Amsterdam, The Netherlands*

7 ^b*Physikalisches Institut, University of Bonn, Nussallee 12, 53115 Bonn,*
8 *Germany*

9 **Abstract**

10 A Time Projection Chamber (TPC) module with 32 GridPix chips was con-
11 structed and the performance was measured using data taken in a testbeam at
12 DESY in 2021. The GridPix chips each consist of a Timepix3 chip with inte-
13 grated amplification grid and have a high efficiency to detect single ionisation
14 electrons. In the testbeam setup, the module was placed in between two sets of
15 Mimosas26 silicon detector planes that provided external high precision tracking
16 and the whole detector setup was slid into the PCMag magnet at DESY.
17 The analysed data were taken at electron beam momenta of 5 and 6 *GeV/c* and
18 at magnetic fields of 0 and 1 Tesla(T).

19 The result for the transverse diffusion coefficient D_T is $287 \mu\text{m}/\sqrt{cm}$ at $B =$
20 0 T and D_T is $121 \mu\text{m}/\sqrt{cm}$ at $B = 1 \text{ T}$. The longitudinal diffusion coefficient
21 D_L is measured to be $268 \mu\text{m}/\sqrt{cm}$ at $B = 0 \text{ T}$ and $252 \mu\text{m}/\sqrt{cm}$ at $B = 1$
22 T . Results for the tracking systematical uncertainties in xy (pixel plane) were
23 measured to be smaller than $13 \mu\text{m}$ with and without magnetic field. The
24 tracking systematical uncertainties in z (drift direction) were smaller than 15
25 μm ($B = 0 \text{ T}$) and $20 \mu\text{m}$ ($B = 1 \text{ T}$).

26 *Keywords:* Micromegas, gaseous pixel detector, micro-pattern gaseous
27 detector, Timepix, GridPix, pixel time projection chamber

*Corresponding author. Telephone: +31 20 592 2000
Email address: s01@nikhef.nl (P.M. Kluit)

28 1. Introduction

29 Earlier publications on a single chip [1] and four chip (quad) GridPix detec-
30 tors [2] showed the potential of the GridPix technology and the large range of
31 applications for these devices [3]. In particular, it was demonstrated that single
32 ionisation electrons can be detected with high efficiency and great precision,
33 allowing excellent 3D track position measurements and particle identification
34 based on the number of electrons and clusters.

35 As a next step towards a Pixel Time Projection Chamber for a future col-
36 lider experiment [4], [5], a module consisting of 32 GridPix chips based on the
37 Timepix3 chip was constructed.

38 A GridPix detector consists of a CMOS pixel Timepix3 chip [6] with inte-
39 grated amplification grid added by Micro-electromechanical Systems (MEMS)
40 postprocessing techniques. The Timepix3 chip can be operated with a low
41 threshold of $515 e^-$, and has a low equivalent noise charge of about $70 e^-$. The
42 GridPix single chip and quad detectors have a very fine granularity of 55×55
43 μm^2 and a high efficiency to detect single ionisation electrons.

44 Based on the experience gained with these detectors a 32 GridPix chip mod-
45 ule - consisting of 8 quads - was built. A drift box defining the electric field
46 and gas envelop was constructed. A readout system for up to 128 chips with 4
47 multiplexers readout by one speedy pixel detector readout SPIDR board [7] [8]
48 was designed. After a series of tests using the laser setup [9] and cosmics in the
49 laboratory at Nikhef, the detector was taken to DESY for a two week testbeam
50 campaign.

51 At DESY the 32 chip detector was placed in between two sets of Mimosas26
52 silicon detector planes and mounted on a movable stage. The whole detector
53 setup was slid into the centre of the PCMAG magnet at DESY. A beam
54 trigger was provided by scintillator counters. The data reported here were taken
55 at different stage positions and electron beam momenta of 5 and 6 GeV/c and
56 at magnetic fields of 0 and 1 T. The performance of the 32 GridPix chip module
57 was measured using these data sets.

58 In this paper part I of the results will be presented with the main focus on
59 the detector spatial resolution and tracking performance. A second follow up
60 paper will discuss the dE/dx (or dN/dx) and other results.

61 **2. The 32 GridPix chip module**

62 A 32 GridPix chip module was built using the quad module [2] as a basic
63 building block. The quad module consists of four GridPix chips and is optimised
64 for a high fraction of sensitive area of 68.9%. The external dimensions are 39.60
65 x 28.38 mm. The four chips which are mounted on a cooled base plate (COCA),
66 are connected with wire bonds to a common central 6 mm wide PCB. A 10 mm
67 wide guard electrode is placed over the wire bonds 1.1 mm above the aluminium
68 grids, in order to prevent field distortions of the electric drift field. The guard is
69 the main inactive area, and its dimensions are set by the space required for the
70 wire bonds. On the back side of the quad module, the PCB is connected to a
71 low voltage regulator. The aluminium grids of the GridPixes are connected by
72 80 μm insulated copper wires to a high voltage (HV) filtering board. The quad
73 module consumes about 8W of power of which 2W is used in the LV regulator.

74 Eight quad modules were embedded in a box, resulting in a GridPix module
75 with a total of 32 chips. A schematic 3-dimensional drawing of the detector is
76 shown in Figure 1. A schematic drawing of the quads in the module is shown
77 in Figure 2, where also the beam direction is indicated.

78 The internal dimensions of the box are 79 mm along the x -axis, 192 mm along
79 the y -axis, and 53 mm along the z -axis (drift direction), and it has a maximum
80 drift length (distance between cathode and readout anode) of 40 mm. The drift
81 field is shaped by a series of parallel CuBe field wires of 75 μm diameter with
82 a wire pitch of 2 mm and guard strips are located on all of the four sides of the
83 active area. In addition, six guard wires - shown with dashed lines in Figure
84 2 - are suspended over the boundaries of the chips, where no guard is present,
85 to minimise distortions of the electric drift field. The wires are located at a
86 distance of 1.15 mm from the grid planes, and their potential is set to the drift

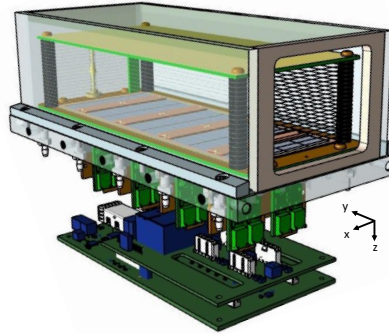


Figure 1: Schematic 3-dimensional render of the 8-quad module detector for illustration purposes.

87 potential at this drift distance. The box has two Kapton $50 \mu\text{m}$ windows to
 88 allow the beam to pass with minimal multiple scattering.

89 The gas volume of 780 ml is continuously flushed at a rate of $\sim 50 \text{ ml/min}$
 90 (about 4 volumes/hour) with premixed T2K TPC gas. This gas is a mixture
 91 consisting of 95% Ar, 3% CF_4 , and 2% iC_4H_{10} suitable for large TPCs because
 92 of the low transverse diffusion in a magnetic field and the high drift velocity.

93 The data acquisition system of the quad module was adopted to allow for
 94 reading out multiple quads. A multiplexer card was developed that handles
 95 four quads or 16 chips and combines the Timepix3 data into one data stream.

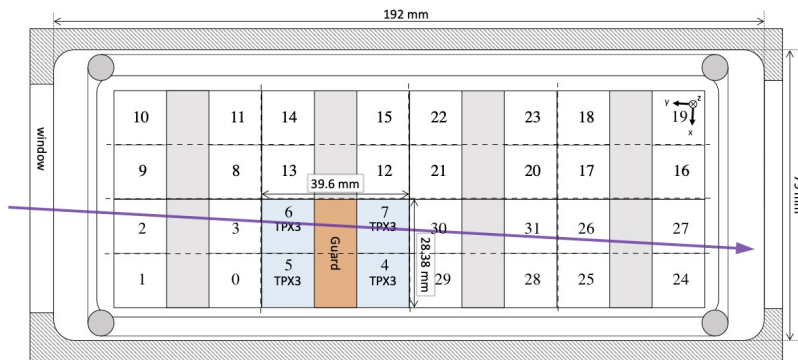


Figure 2: Schematic drawing of the 8-quad module detector with one example quad as viewed from the top of the quads. The chips are numbered and the beam direction is shown in purple.

96 For the 32 GrixPix module two multiplexers are connected to a SPIDR board
97 that controls the chips and readout process. The readout speed per chip is 160
98 Mbps and for the multiplexer 2.56 Gbps this corresponds to a maximum rate of
99 21MHits/s. For each pixel the precise Time of Arrival (ToA) using a 640 MHz
100 TDC and the time over threshold (ToT) are measured.

101 **3. Experimental setup**

102 In preparation of the two weeks DESY testbeam campaign, a support frame
103 was designed to move the 32 chip GridPix module in the plane perpendicular to
104 the beam by a remotely controlled stage such that the whole detector volume
105 could be probed. The module was mounted upside down with respect to figure
106 1 to allow access to the electronics from above. The support frame also held
107 three Mimoso26 silicon detector planes [10] - with an active area of (21.2 mm x
108 10.6 mm) - placed in front of the detector and three Mimoso26 planes behind
109 the detector. At DESY the (Mimoso26) silicon detector planes were provided
110 by the testbeam coordinators. The whole detector setup was slid towards
111 the centre of the PCMAG magnet at the DESY II testbeam facility [10]. A
112 beam trigger was provided by a double scintillator counter coincidence. The
113 data were taken at different stage positions to cover the whole sensitive TPC
114 volume. Runs with electron beam momenta of 5 and 6 GeV/c and at magnetic
115 fields of 0 and 1 T were analysed.

116 A photograph of the detector setup in the PCMAG magnet is shown in
117 Figure 3.

118 The experimental and environmental parametres such as temperature, pres-
119 sure, gas flow, oxyxygen content were measured and logged by a Windows op-
120 erated slow control system. The experimental parametres are summarised in
121 Table 1. The chips were cooled by circulating Glycol through the cooling chan-
122 nels in the module carrier plate. The cooling blocks of the multiplexers were
123 further cooled by blowing pressurised air on them.

124 The data was produced in four main data streams: one stream produced by

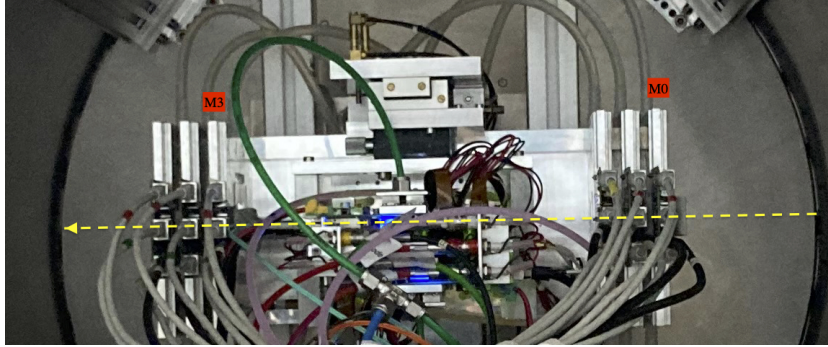


Figure 3: Photo of the detector setup at the centre of the PCMAG magnet. The Mimosa26 planes M0 and M3 are indicated in red as well as the beam direction (yellow). Centrally, the stage positions the TPC module with respect to the beam and the Mimosa26 planes.

Table 1: Overview of the experimental parameters. The ranges indicate the variation over the data taking period

Number of analysed runs at B=0 (1) T	6 (8)
Run duration	10-90 minutes
Number of triggers per run	3-100 k
E_{drift}	280 V/cm
V_{grid}	340V
Threshold	550 e ⁻
Gas temperature	303.3-306.6 K
Pressure	1011 – 1023 mbar
Oxygen concentration	240 - 620 ppm
Water vapour concentration	2000 - 7000 ppm

125 the Mimosa26 Telescope, two data streams by the two Timepix multiplexers and
126 one trigger stream. The double scintillator coincidence provided a trigger signal
127 to the Trigger Logic Unit (TLU) [11] that sends a signal to the telescope readout
128 and the trigger SPIDR. The data acquisition system of the Telescope and trigger
129 SPIDR injected a time stamp into their respective data streams. Hits from the
130 Mimosa26 planes were collected with a sliding window of $-115 \mu\text{s}$ to $230 \mu\text{s}$ of
131 the trigger. The data acquisition of the multiplexer and the trigger SPIDR were
132 synchronised at the start of the run. By comparing the time stamps in these
133 streams, Telescope tracks and TPC tracks could be matched. Unfortunately,
134 the SPIDR trigger had - due to a cabling mistake at the output of the TLU - a
135 common 25nsec time jitter.

136 After a short data taking period one of the chips (nr 11) developed a short
137 circuit and the HV on the grid of the chip was disconnected. After the testbeam
138 data taking period the module was repaired in the clean room in Bonn.

139 4. Analysis

140 4.1. Telescope Track reconstruction procedure

141 The data of the Telescope is decoded and analysed using the Corryvreckan
142 software package [12]. The track model used for fitting was the General Broken
143 Lines (GBL) software [14]. The code was extended and optimised to fit curved
144 broken lines for the data with magnetic field. The telescope planes were itera-
145 tively aligned using the standard alignment software provided by the package.
146 The single point Mimosa26 resolution is $4 \mu\text{m}$ in x and $6 \mu\text{m}$ in z (drift direction)
147 [10].

148 Telescope tracks were selected with at least 5 out of the 6 planes on the track
149 and a total χ^2 of better than 25 per degree of freedom. The uncertainties on the
150 Telescope track prediction in the middle of the GridPix module are dominated
151 by multiple scattering. The amount of multiple scattering was estimated by
152 comparing the predictions from the two telescope arms for $6 \text{ GeV}/c$ tracks at B
153 $= 0 \text{ T}$. The expected uncertainty in x and z is $26 \mu\text{m}$ on average.

154 *4.2. TPC Track reconstruction procedure*

155 GridPx hits are selected requiring a minimum time over threshold ToT of
156 0.15 μ s. The drift time is defined as the measured time of arrival minus the
157 trigger time recorded in the trigger SPIDR data stream minus a fixed t_0 (the
158 drift time at zero drift). The drift time was corrected for time walk [2] using
159 the measured time over threshold (ToT in units of μ s) and the formula (1):

$$\delta t = \frac{18.6(ns\mu s)}{\text{ToT} + 0.1577(\mu s)}. \quad (1)$$

160 Furthermore, small time shift corrections - with an odd-even and a 16x2 pixels
161 structure - coming from the TPX3 clock distribution were extracted from the
162 data and applied.

163 The z drift coordinate was calculated as the product of the drift time and the
164 drift velocity. This implies that $z_{\text{drift}} = -z$ as defined in figure 1. GridPix hits
165 outside an acceptance window of 30 mm wide in x and 15 mm wide in z were
166 not used in the track finding and reconstruction. Based on a Hough transform
167 an estimate of the TPC track position and angles in the middle of the module
168 (at $y = 1436$ pixels) was obtained. This estimate was used to collect the hits
169 around the TPC track and fit the track parameters. For this fit a straight line
170 ($B = 0$ T) or a quadratic track $B = 1$ T model was used. In the fit, the expected
171 uncertainties per hit σ_x and σ_z were used. The fit was iterated three times to
172 perform outlier removal at respectively 10, 5 and 2.5 sigma level. A TPC track
173 was required to have a least 100 hits in each multiplexer. At least 25% of the
174 total number of hits should be on track and the χ^2 per degree of freedom had
175 to be less than 3 in xy and zy. All track parameters were expressed at a plane
176 in the middle of the TPC.

177 The calibration and alignment of the detector was done using high quality
178 tracks for which the track selections are summarised in table 2.

179 The drift velocity was calibrated per run by fitting a linear function to the z
180 (predicted from the Telescope track at the measured TPC hit position) versus
181 the measured drift time in the TPC. For the $B = 0$ T runs it varies between

Table 2: Table with track/event selection cuts

Track/Event Selection
$ x_{\text{TPC}} - x_{\text{Telescope}} < 0.3 \text{ mm}$
$ z_{\text{TPC}} - z_{\text{Telescope}} < 2 \text{ mm}$
$ dx/dy_{\text{TPC}} - dx/dy_{\text{Telescope}} < 4 \text{ mrad}$
$ dz/dy_{\text{TPC}} - dz/dy_{\text{Telescope}} < 2 \text{ mrad}$

182 61.6 and 63.0 $\mu\text{m}/\text{ns}$. For the $B = 1 \text{ T}$ runs it is between 57.2 and 59.1 $\mu\text{m}/\text{ns}$.
 183 The variation comes mainly from the changes in the relative humidity of the
 184 gas volume due to small leaks.

185 The individual TPX3 chips were iteratively aligned fitting a shift in x (z drift)
 186 and two slopes $dx(z \text{ drift})/d \text{ row}(\text{column})$. The alignment was done per run,
 187 because the detector was moved in x and/or z for each run. The fitted slopes
 188 were also corrected for small shifts and rotations (3D) in the nominal chip
 189 position.

190 An example event run 6916 without B field with a TPC and a telescope
 191 track is shown in figure 4. The TPC is located between $y = 0$ and 2872 pixels.
 192 Three Mimosas26 planes are located at $y < -1000$ and three at $y > 4000$ pixels.

193 5. Hit resolutions

194 In order to study the single electron resolution for the data with and without
 195 magnetic field, additional selections on the Telescope and TPC tracks were
 196 applied. Due to the trigger time jitter of 25 nsec (corresponding to 1.5 mm
 197 drift), the prediction of the telescope track in z must be used as the reference for
 198 z . Secondly, the z hits of the TPC track were fitted to correct for the common
 199 time shift and the z residuals were calculated with respect to the fitted TPC
 200 track. In the xy plane the residuals of TPC hits with respect to the telescope
 201 track were used to extract the single electron resolution in xy . For the resolution
 202 studies runs at three different z stage positions of the TPC were selected where

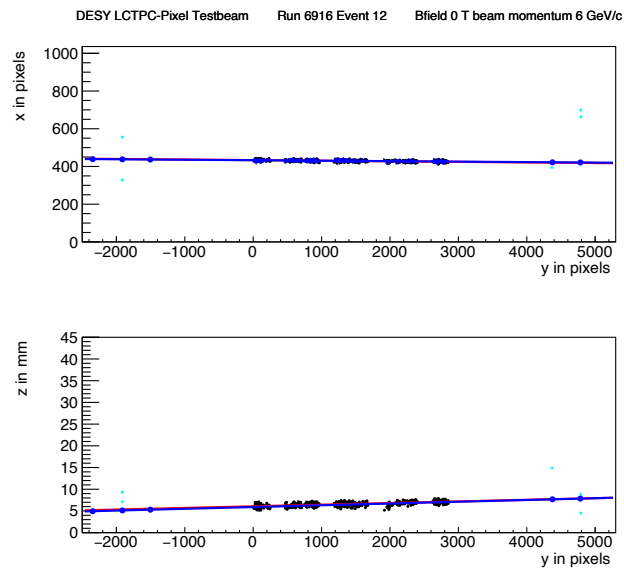


Figure 4: An event display for run 6916 without B field, with in total 1293 TPC hits (black dots) in the precision plane (x,y) and driftplane (z drift,y). The fitted TPC track (red line) with 1130 hits on track and the telescope track (blue line) with 5 Mimosa26 planes (blue hits) on track are shown. In green the off track Mimosa26 hits are shown.

203 the beam gave hits in the central chips. The data of 14 central chips (9, 12, 21,
 204 20, 17, 16, 2, 3, 6, 7, 30, 31, 26 and 27) was used. Two chips (8 and 13) were
 205 left out because of the E field deformations caused by the short circuit in chip
 206 11.

207 5.1. Hit resolutions in the pixel plane

208 The resolution of the hits in the pixel plane (xy) was measured as a function
 209 of the predicted drift position (z_{drift}). Only hits are used crossing the fiducial
 210 region defined by the central core of the beam and staying 20 pixels away from
 211 the chip edges. The resolution for the detection of ionisation electrons σ_x is
 212 given by:

$$\sigma_x^2 = \frac{d_{\text{pixel}}^2}{12} + d_{\text{track}}^2 + D_T^2(z_{\text{drift}} - z_0), \quad (2)$$

213 where d_{pixel} is the pixel pitch size, d_{track} the uncertainty from the track predic-
 214 tion, z_0 is the position of the grid, and D_T is the transverse diffusion coefficient.
 215 The resolution at zero drift distance $d_{\text{pixel}}/\sqrt{12}$ was fixed to 15.9 μm and d_{track}
 216 to 30 μm for $B = 0$ T and 42 μm for $B = 1$ T data. The uncertainty of the track
 217 prediction was measured and is larger than the Mimosa plane resolution because
 218 of multiple scattering in the sensor and in the entrance and exit windows.

219 The expression (2) - leaving z_0 and D_T as free parameters - is fitted to the B
 220 = 0 T data shown in Figure 5. The fit gives a transverse diffusion coefficient D_T
 221 of 287 $\mu\text{m}/\sqrt{cm}$ with negligible statistical uncertainty. The measured value is in
 222 agreement with the value of 287 $\mu\text{m}/\sqrt{cm} \pm 4\%$ predicted by the gas simulation
 223 software Magboltz [15]. The values of the diffusion coefficients depend on the
 224 humidity that was not precisely measured during the testbeam. The humidity
 225 strongly affects the drift velocity. Therefore the drift velocity prediction from
 226 Magboltz was used to determine the water content per run and predictions for
 227 the diffusion coefficients could be obtained.

228 A fit to the $B = 1$ T data, also shown in Figure 5, gives a transverse diffu-
 229 sion coefficient D_T of 121 $\mu\text{m}/\sqrt{cm}$ with negligible statistical uncertainty. The
 230 measured value is in agreement with the value of 119 $\mu\text{m}/\sqrt{cm} \pm 2\%$ predicted
 231 by Magboltz.

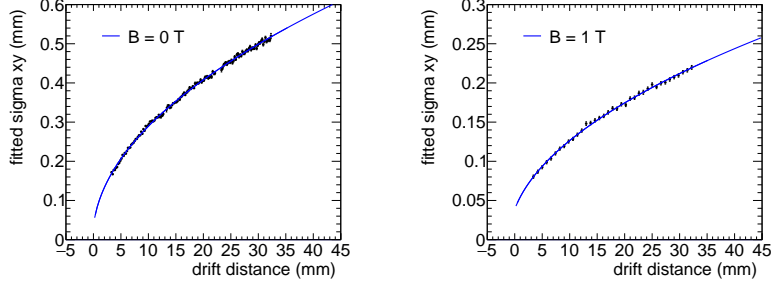


Figure 5: Measured hit resolution in the pixel plane (black points) fitted with the resolution function according to equation (2) (blue line).

232 *5.2. Hit resolution in the drift plane*

233 The resolution for the detection of ionisation electrons σ_z in the drift plane
 234 is given by:

$$\sigma_z^2 = \sigma_{z0}^2 + d_{\text{track}}^2 + D_L^2(z_{\text{drift}} - z_0), \quad (3)$$

235 where σ_{z0} is the resolution at zero drift distance, d_{track} the expected track
 236 uncertainty and D_L the longitudinal diffusion constant. Only tracks crossing
 237 the fiducial region were accepted and hits with a ToT value above $0.6 \mu\text{s}$ were
 238 selected. Because of the time jitter, the fitted TPC track is used for the drift
 239 residuals. For z_{drift} the Telescope prediction at the hit was used. The expected
 240 uncertainty on the Telescope track prediction is $25 \mu\text{m}$.

241 The expression (3) - leaving σ_{z0} and D_L as free parameters - is fitted to
 242 the $B = 0 \text{ T}$ data shown in Figure 6. The value of z_0 was fixed to the result
 243 of the fit in the xy plane. The value of σ_{z0} was measured to be $138 \mu\text{m}$. The
 244 longitudinal diffusion coefficient D_L was determined to be $(265 \pm 1) \mu\text{m}/\sqrt{\text{cm}}$,
 245 which is higher than the expected value $(236 \pm 3) \mu\text{m}/\sqrt{\text{cm}}$ from a Magboltz
 246 calculation [15].

247 A fit to the $B = 1 \text{ T}$ data shown in Figure 6 gives a longitudinal diffusion
 248 coefficient D_L of $(250 \pm 2) \mu\text{m}/\sqrt{\text{cm}}$. The measured value is in agreement with
 249 the value of $(245 \pm 4) \mu\text{m}/\sqrt{\text{cm}}$ predicted by Magboltz. The fitted value of σ_{z0}
 250 was $133 \mu\text{m}$.

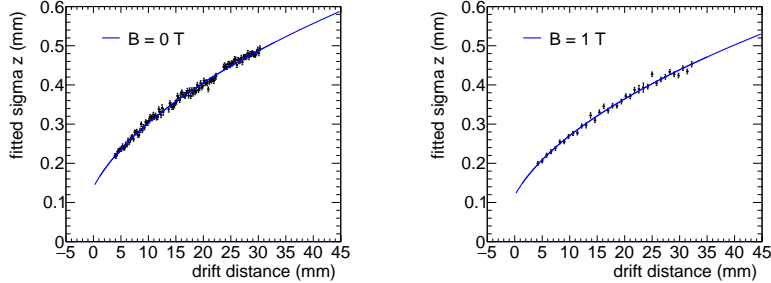


Figure 6: Resolution in the drift plane for hits with a ToT above $0.60 \mu\text{s}$. The data are fitted with the expression of equation (3).

251 5.3. Deformations in the pixel and drift plane

252 It is important to measure possible deformations in the pixel (xy) and drift
 253 (z) plane to quantify the tracking precision. For the construction of a large Pixel
 254 TPC, deformations in the pixel plane deformation should be controlled to better
 255 than typically $20 \mu\text{m}$ because these affect the momentum resolution. The mean
 256 residuals in the pixel and drift planes are shown in Figure 7 for the $B = 0 \text{ T}$
 257 data set using a large set of runs to cover the whole module. The residuals were
 258 calculated with respect to the Telescope track prediction. Because of limited
 259 statistics bins were grouped into 8×16 pixels. Bins with less than 100 hits are
 260 left out and residuals larger (smaller) than $+(-)100 \mu\text{m}$ are shown in red (blue).

261 A few critical areas can be observed in figure 7: the region around chip 11
 262 is affected (chips 14, 8 and 13), because the grid of chip 11 was disconnected.
 263 Deformations are present at the four corners of the drift box (chips 1, 10, 19 and
 264 24) and close to the upper corner edge (chip 16) of the drift box. These come
 265 from inhomogenities in the drift field near the supporting pillars, the field wires
 266 are too close to the chip to provide a constant electric field. It was concluded
 267 that for the deformation results the hits of these nine chips have to be removed.
 268 The track fit was redone leaving these hits out of the fit, such that they could
 269 not bias and affect the results.

270 In order to reduce the statistical fluctuations and quantify the tracking pre-

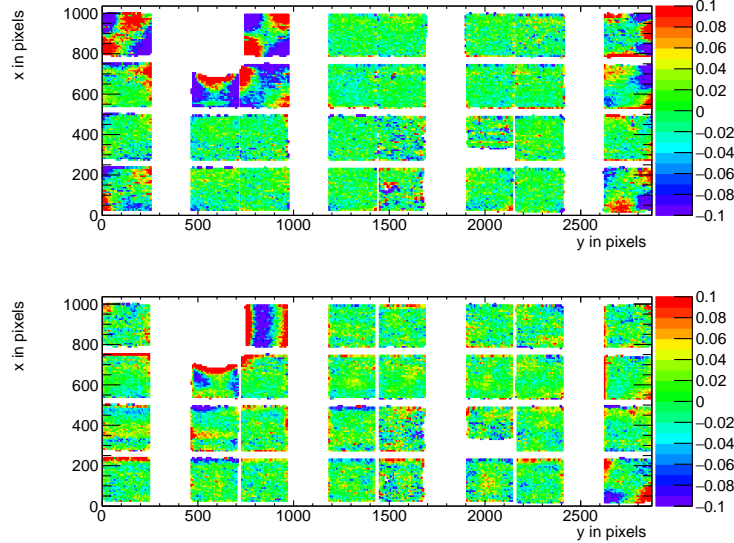


Figure 7: Mean residuals (in mm) in the pixel (top) and drift (bottom) plane for $B = 0$ T data at the expected hit position.

271 cision, the module was regrouped in four 256x256 pixel planes put side by side
 272 on the horizontal axis, as shown in figure 8. Bins have a size of 16x16 pixels and
 273 bins with less than 1000 entries are not shown. A bias in the mean residual at
 274 the edge of the chips is expected to be present for an ideal detector because of
 275 the finite coverage and the diffusion in the drift process. Due to the presence of
 276 the dike pixels at the edge of the chip became covered and inefficient. Therefore
 277 the region near the edge of 5 pixels was removed. For the drift coordinate a
 278 region of 10 pixels was removed. The total number of measurements (bins) in
 279 xy is 895 and in z 892. One can observe that in the module plane no clear sys-
 280 tematic deviations are present and conclude that the guard wire voltages were
 281 on average well tuned. Note that in the quad module we had no guard wires
 282 and deformation corrections had to be applied [2]. The r.m.s. of the distribu-
 283 tion of the measured mean residual over the surface in the pixel plane is $11 \mu\text{m}$
 284 and in the drift plane $15 \mu\text{m}$. Similarly, regrouping the module in four planes
 285 of 256x256 pixels putting them on top of each other vertically, yielded a r.m.s.

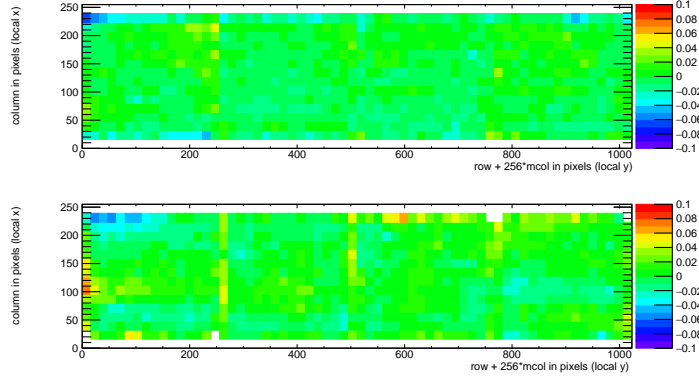


Figure 8: Mean residuals (in mm) in the pixel (top) and drift plane (bottom) for $B = 0$ T data at the regrouped expected hit position.

286 in the pixel plane of $13 \mu\text{m}$ and $13 \mu\text{m}$ in the drift coordinate. The expected
 287 statistical error in xy is $4 \mu\text{m}$ and in z $5 \mu\text{m}$.

288 In the $B = 1$ T data set, the electrons will drift mainly along the magnetic
 289 field lines. Deformations are in that case due to e.g. the non-alignment of the
 290 electric and magnetic field, giving ExB effects. Unfortunately, the statistics of
 291 the Telescope tracks that have a matched TPC track was insufficient and did
 292 not cover the full TPC module plane. Therefore the larger statistics of matched
 293 and unmatched TPC tracks was used. TPC tracks were required to pass angular
 294 selection cuts (dx/dy between -40 and -20 mrad and dz/dy between 0 and 14
 295 mrad) and a momentum cut ($p > 2 \text{ GeV}/c$ and $q < 0$).

296 The mean residuals in the pixel and drift planes are shown in figure 9 for
 297 the $B = 1$ T data set using a large set of runs to cover the whole module. The
 298 residuals were calculated with respect to the TPC track prediction. Because of
 299 limited statistics bins were grouped into 8×16 pixels. Bins with less than 100
 300 hits are left out and residuals larger (smaller) than $+(-)100 \mu\text{m}$ are shown in
 301 red (blue).

302 In figure 9 the critical areas discussed above - around chip 11, the four corner
 303 chips and chip 16 in the upper corner edge - can be clearly observed. For the
 304 deformation results the hits of these nine chips have to be removed. The TPC

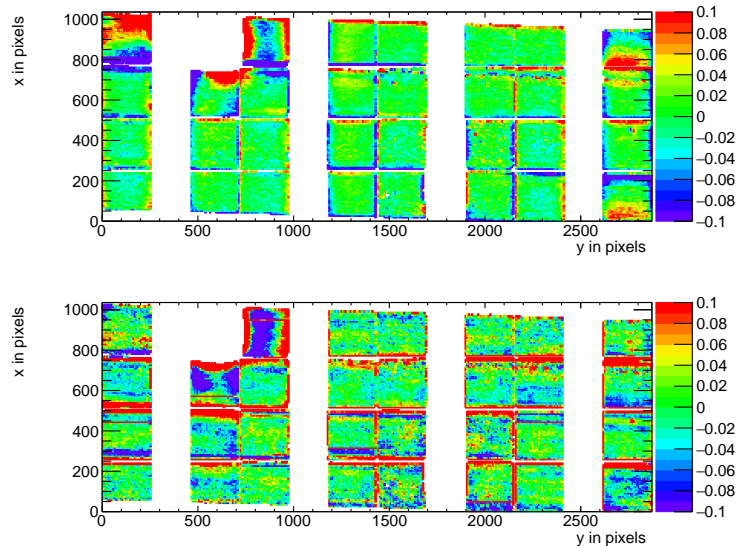


Figure 9: Mean residuals in the pixel and drift plane for $B = 1$ T data at the expected hit position.

305 track fit was redone leaving these hits out of the fit, thus that they could
 306 not bias and affect the results. The TPC plane is well covered, although one
 307 can observe that due to the angle of the beam in the xy plane the chips in the
 308 upper right and lower left corners are not fully covered.

309 In order to reduce the statistical fluctuations and quantify the tracking pre-
 310 cision, the module was regrouped in four 256x256 pixel planes put side by side
 311 on the horizontal axis, as shown in figure 10. Bins have a size of 16x16 pix-
 312 els and bins with less than 1000 entries are not shown. Similar to the no-field
 313 deformations studies, acceptance cuts had to be applied. The region near the
 314 edge of 16 pixels (columns) was removed. For the drift coordinate in addition
 315 a region of 10 pixels (rows) was removed. The total number of measurements
 316 (bins) in xy is 896 and in z 896. One can observe that in the module plane no
 317 clear systematic deviations are present. The r.m.s. of the distribution of the
 318 measured mean residual over the surface in the pixel plane is $13 \mu\text{m}$ and in the
 319 drift plane $19 \mu\text{m}$. Similarly, regrouping the module in four planes of 256x256

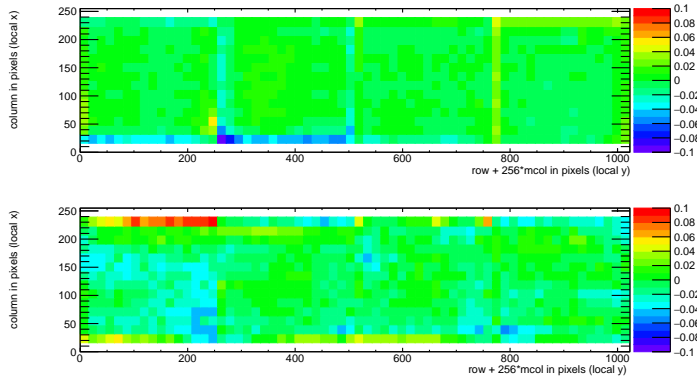


Figure 10: Mean residuals in the pixel and drift plane for B= 1T data at the regrouped expected hit position.

320 pixels side by side vertically, yielded a r.m.s. in the pixel plane of $11 \mu\text{m}$ and
 321 $20 \mu\text{m}$ in the drift coordinate. The expected statistical error in xy is $2 \mu\text{m}$ and
 322 in z $3 \mu\text{m}$.

323 5.4. Tracking resolution

324 A selected TPC track in the B = 0 T data has on average 1000 hits. The
 325 tracking precision in the middle of the TPC was derived on a track-by-track bias
 326 and found to be on average $9 \mu\text{m}$ in the precision plane and $13 \mu\text{m}$ in z. The
 327 angular resolution in dx/dy was on average 0.19 mrad and for dz/dy 0.25 mrad.
 328 It is clear that the position resolution in the TPC in the precision and drift
 329 coordinates is impressive for a track length of (only) 158 mm. The values are
 330 smaller than the uncertainty on the track prediction from the silicon telescope
 331 of $26 \mu\text{m}$ on average that is dominated by multiple scattering.

332 6. Single electron efficiency

333 The distribution of the number of TPC track hits per chip - without requiring
 334 a matched Telescope track - are shown in figure 11 for the data without magnetic
 335 field and for the B = 1 T data. The B = 0 T data analysis selects the central

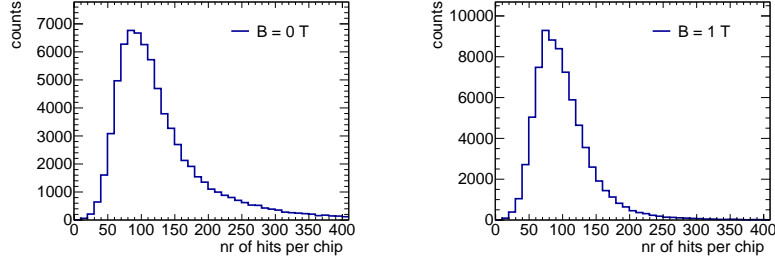


Figure 11: Distribution of the number of track hits per per chip for $B = 0$ T (left) $B = 1$ T data.

336 chips 2,6,7,9,16,17,26 and 27. The $B = 1$ T data analysis selects the same chips
 337 plus chips 12,13,20 and 21.

338 The mean number of hits is measured to be 124 and 89 in the $B = 0$ T and
 339 1 T data sets respectively. The most probable values are respectively 87 and
 340 64. Note that the $B = 0$ T data have a much larger Landau-like tail than the
 341 1 T data. Also the fluctuations in the core of the distribution are larger. The
 342 mean time over threshold is $0.68 \mu\text{s}$ for the $B = 0$ T and $0.86 \mu\text{s}$ at a $B = 1$
 343 T data. This means that the deposited charge per pixel is smaller for the 0 T
 344 data. The most probable value for the total deposited charge is similar for both
 345 data sets. The mean number of hits is in agreement with the predictions of [13]
 346 106 electron-ion pairs for a $6 \text{ GeV}/c$ electron at $B = 0$ T, crossing 236 pixels or
 347 12.98 mm and a detector running at 85% single electron efficiency.

348 7. Conclusion and outlook

349 A Time Projection Chamber module with 32 GridPix chips was constructed
 350 and the performance was measured using data taken in a testbeam at DESY
 351 in 2021. The analysed data were taken at electron beam momenta of 5 and 6
 352 GeV/c and at magnetic fields of 0 and 1 T.

353 The result for the transverse diffusion coefficient D_T is $287 \mu\text{m}/\sqrt{cm}$ at $B =$
 354 0 T and D_T is $121 \mu\text{m}/\sqrt{cm}$ at $B = 1$ T. The longitudinal diffusion coefficient
 355 D_L is measured to be $268 \mu\text{m}/\sqrt{cm}$ at $B = 0$ T and $252 \mu\text{m}/\sqrt{cm}$ at $B = 1$ T.

356 Results for the tracking systematical uncertainties in xy were measured to be
357 smaller than $13\ \mu\text{m}$ with and without magnetic field. The tracking systematical
358 uncertainties in z were smaller than $15\ \mu\text{m}$ ($B = 0\ \text{T}$) and $20\ \mu\text{m}$ ($B = 1\ \text{T}$).

359 The mean number of hits is in agreement with the predictions of [13] and a
360 detector running at 85% single electron efficiency.

361 Not all data were analysed and users are welcome to study them using the
362 data sets on available on the Grid.

363 The GridPix detector will be further tested and developed in view of a
364 TPC that will be installed in a heavy ion experiment at the EIC. A follow up
365 paper is in preparation on the measured dE/dx or dN/dx resolution and other
366 performance topics.

367 **Acknowledgements**

368 This research was funded by the Netherlands Organisation for Scientific Re-
369 search NWO. The authors want to thank the support of the mechanical and
370 electronics departments at Nikhef and the detector laboratory in Bonn. The
371 measurements leading to these results have been performed at the Test Beam
372 Facility at DESY Hamburg (Germany), a member of the Helmholtz Association
373 (HGF).

374 **References**

- 375 [1] C. Ligtenberg, et al., Performance of a GridPix detector based on the
376 Timepix3 chip, Nucl. Instrum. Meth. A 908 (2018) 18–23. [arXiv:1808.04565](#), [doi:10.1016/j.nima.2018.08.012](#).
- 377
- 378 [2] C. Ligtenberg, et al., Performance of the GridPix detector quad, Nucl.
379 Instrum. Meth. A 956 (2020) 163331. [arXiv:2001.01540](#), [doi:10.1016/j.nima.2019.163331](#).
- 380
- 381 [3] J. Kaminski, Y. Bilevych, K. Desch, C. Krieger, M. Lupberger, GridPix de-
382 tectors - introduction and applications, Nucl. Instrum. Meth. A845 (2017)
383 233–235. [doi:10.1016/j.nima.2016.05.134](#).

- 384 [4] C. Ligtenberg, A GridPix TPC readout for the ILD experiment at the
385 future International Linear Collider, Ph.D. thesis, Free University of
386 Amsterdam (2021).
387 URL [https://www.nikhef.nl/pub/services/biblio/theses_pdf/
388 thesis_C_Ligtenberg.pdf](https://www.nikhef.nl/pub/services/biblio/theses_pdf/thesis_C_Ligtenberg.pdf)
- 389 [5] M. Lupberger, Y. Bilevych, H. Blank, D. Danilov, K. Desch, A. Hamann,
390 J. Kaminski, W. Ockenfels, J. Tomtschak, S. Zigann-Wack, Toward the
391 Pixel-TPC: Construction and Operation of a Large Area GridPix Detector,
392 IEEE Trans. Nucl. Sci. 64 (5) (2017) 1159–1167. doi:10.1109/TNS.2017.
393 2689244.
- 394 [6] T. Poikela, J. Plosila, T. Westerlund, M. Campbell, M. De Gaspari,
395 X. Llopart, V. Gromov, R. Kluit, M. van Beuzekom, F. Zappone,
396 V. Zivkovic, C. Brezina, K. Desch, Y. Fu, A. Kruth, Timepix3: a 65K
397 channel hybrid pixel readout chip with simultaneous ToA/ToT and sparse
398 readout, JINST 9 (05) (2014) C05013.
399 URL <http://stacks.iop.org/1748-0221/9/i=05/a=C05013>
- 400 [7] J. Visser, M. van Beuzekom, H. Boterenbrood, B. van der Heijden, J. I.
401 Muñoz, S. Kulis, B. Munneke, F. Schreuder, SPIDR: a read-out system for
402 Medipix3 & Timepix3, Journal of Instrumentation 10 (12) (2015) C12028.
403 doi:10.1088/1748-0221/10/12/C12028.
- 404 [8] B. van der Heijden, J. Visser, M. van Beuzekom, H. Boterenbrood, S. Kulis,
405 B. Munneke, F. Schreuder, SPIDR, a general-purpose readout system for
406 pixel ASICs, JINST 12 (02) (2017) C02040. doi:10.1088/1748-0221/12/
407 02/C02040.
- 408 [9] F. Hartjes, A diffraction limited nitrogen laser for detector calibration in
409 high energy physics, Ph.D. thesis, University of Amsterdam (1990).
410 URL [https://www.nikhef.nl/pub/services/biblio/theses_pdf/
411 thesis_F_Hartjes.pdf](https://www.nikhef.nl/pub/services/biblio/theses_pdf/thesis_F_Hartjes.pdf)

- 412 [10] R. Diener et al., The DESY II test beam facility, Nuclear Instruments
413 and Methods in Physics Research. Section A: Accelerators, Spectrometers,
414 Detectors and Associated Equipment 922 (2019) 265–286. [arXiv:1807.](#)
415 [09328](#), [doi:10.1016/j.nima.2018.11.133](#).
- 416 [11] P. Baesso, D. Cussans, J. Goldstein, The AIDA-2020 TLU: a flexible trigger
417 logic unit for test beam facilities, Journal of Instrumentation 14 (09) (2019)
418 P09019–P09019. [arXiv:2005.00310](#).
419 URL <https://doi.org/10.1088/1748-0221/14/09/p09019>
- 420 [12] D. Dannheim, K. Dort, L. Huth, D. Hynds, I. Kremastiotis, J. Kröger,
421 M. Munker, F. Pitters, P. Schütze, S. Spannagel, T. Vanat, M. Williams,
422 Corryvreckan: a modular 4d track reconstruction and analysis software
423 for test beam data, Journal of Instrumentation 16 (03) (2021) P03008.
424 [doi:10.1088/1748-0221/16/03/p03008](#). [arXiv:2011.12730](#).
425 URL <https://doi.org/10.1088/1748-0221/16/03/p03008>
- 426 [13] R. Veenhof, Garfield - simulation of gaseous detectors, version 9, Reference
427 W5050 (1984-2010).
428 URL <https://garfield.web.cern.ch>
- 429 [14] C. Kleinwort, General broken lines as advanced track fitting method, Nu-
430 clear Instruments and Methods in Physics Research Section A: Accelera-
431 tors, Spectrometers, Detectors and Associated Equipment 673 (2012) 107–
432 110. [doi:10.1016/j.nima.2012.01.024](#).
- 433 [15] S. F. Biagi, Monte Carlo simulation of electron drift and diffusion in count-
434 ing gases under the influence of electric and magnetic fields, Nucl. Instrum.
435 Meth. A421 (1-2) (1999) 234–240. [doi:10.1016/S0168-9002\(98\)01233-9](#).
436 URL <https://magboltz.web.cern.ch/magboltz>